ERDC/CHL CHETN-I-92
October 2016

US Army Corps of Engineers®

Importance of Antecedent Beach and Surf-Zone Morphology to Wave Runup Predictions

by Katherine L. Brodie

PURPOSE: The purpose of this Coastal and Hydraulics Engineering Technical Note (CHETN) is to present results of initial research on an investigation into the forcing parameters of wave runup on an intermediate, barred beach using innovative observational techniques. A brief overview of the technology and processing used to extract wave data from the terrestrial laser scanner is presented, and relationships between runup, foreshore change, and wave characteristics at the base of the foreshore are investigated. In addition, discussion is provided concerning the implications and causes of foreshore morphology evolution and observed tidal oscillations in wave observations at the base of the foreshore. A new equation for runup is also presented. It is based on a mix of wave parameters measured at the base of the foreshore and from offshore. This new equation explains 73% of the variance in wave runup observations. The results of this work suggest that knowledge of both the surf-zone and beach morphology prior to an approaching storm is critical for accurate predictions of runup inundation and erosion.

INTRODUCTION: Accurately predicting beach evolution and coastal inundation during storms requires models that correctly predict wave runup and swash-zone processes, the principle drivers of sediment exchange between the beach and surf-zone (Masselink and Hughes 1998), as well as up-to-date antecedent data to initialize conditions. Recent research quantified a relationship between spatial variations in the amount of wave-breaking within the inner surf-zone and the volume of erosion of the sub-aerial beach during a nor'Easter along 10 km of the northern Outer Banks (Brodie and McNinch 2011). Specifically, regions with increased wave breaking in the inner-surf zone (due to the presence of an inner bar) were found to correlate with regions of decreased erosion, perhaps due to reduced wave energy impinging on the beach. In this technical note, results are presented which suggest the correlation may be explained by the effect that wave dissipation over variable morphology in the surf-zone has on the resultant energy available for wave runup, and therefore inundation and erosion of the beach. In order to investigate the physical drivers of wave runup in the field during storm conditions, an automated terrestrial laser scanner was mounted above the dune (Figure 1A) to continuously measure the free surface profile of the beach and water surface. This unique data collection technique enabled simultaneous collection of data on foreshore evolution, runup, and inner-surf-zone wave and water level characteristics along a narrow cross-shore transect (Figure 1B, Brodie et al. 2010); all of the parameters forced wave-driven runup.

Observations of the beach during high-energy conditions and post-storm wrack-lines have long suggested that maximum water levels during storms are often much higher than measured water levels in the surf-zone and can vary significantly alongshore. A growing body of literature suggests that comparing maximum and mean water levels reached during storms with variations in beach and dune morphology will therefore be a good predictor of areas of the coast that are particularly susceptible to coastal erosion and damage during extreme storms (Sallenger, Jr. 2000; Stockdon et al. 2007; Plant et al. 2010). While these storm-impact models perform better than random models (54% accuracy compared to 33%), there is clearly room for improvement (Stockdon et al. 2007).

Total water levels reached during storms are calculated as the sum of astronomical tide, surge, wave-driven setup, and wave runup. Wave-driven setup is defined as the super-elevation of the mean water

level due to cross-shore gradients in radiation stress induced by wave breaking (Longuet-Higgins and Stewart 1964). It is often measured at the shoreline by averaging the elevation of the swash over a given time period, (ηr) (Stockdon et al. 2006). Wave runup is the time-varying elevation of the most shoreward swash excursion on the foreshore, with maximum runup often defined as the 2% exceedence elevation of runup swash events over a given time period (Stockdon et al 2006; Holman 1986).

Relationships between runup and setup and important forcing variables, such as beach foreshore slope, offshore wave height and period (wavelength), and surf-zone morphology, have been the focus of many studies, and the relationships found often varied depending on the type of beach studied (Holland et al. 1995; Raubenheimer and Guza 1996; Guza and Thornton 1981; Holman and Sallenger, Jr. 1985; Nielsen and Hanslow 1991; Ruessink et al. 1998; Ruggiero 2004). Stockdon et al. (2006) provide a review of the aforementioned relationships and propose an empirical relationship between the 2% exceedence elevation of runup (R_2) and foreshore beach slope (βf), local wave height (e.g., 10 m water depth) reverse-shoaled to its deepwater equivalent (Ho), and deep-water wavelength (Lo):

$$R_2 = 1.1\left\{0.35\beta_f\left(H_0L_0\right)^{\frac{1}{2}} + \frac{\left[H_0L_0\left(0.563\beta_f^2 + 0.004\right)\right]^{\frac{1}{2}}}{2}\right\} \quad \text{Eq. 1}$$

While Equation 1 is easy to calculate for given boundary conditions (βf, Ho, Lo), accurately defining βf may be difficult, particularly on intermediate beaches where profiles often have cross-shore variations in slope and can change on the timescale of hours (Holland and Puleo 2001). Though Equation 1 is used extensively in the field, a surprising amount of scatter remains unexplained in runup data sets. Melby (2012) also reviewed a number of empirical and numerical modeling approaches for predicting wave runup. He found that the numerical model CSHORE (Kobayashi 2009) provided similar skill to the Stockdon relationship but provided significantly poorer results on dissipative beaches. For both approaches, he noted that outdated, forcing morphological data may have skewed results.

Total energy in the swash is dependent upon contributions from both the incident swell band (defined here as frequencies (f), 0.05Hz < f <0.25Hz) and infragravity band waves (f < 0.05Hz). On intermediate and reflective beaches, the incident band is generally more dominant in swash spectra (Raubenheimer and Guza 1996; Holland and Holman 1993), whereas on dissipative beaches or during storm conditions, the infragravity band tends to dominate swash variance (Ruessink et al. 1998; Ruggiero 2004). Recent work by Guedes et al. (2011) suggests that the tide level may have an important effect on swash statistics (including R_2), particularly at intermediate beaches through the modulation of incident band wave breaking over sandbars. This dependence on conditions within the inner surf-zone suggests that wave parameters observed outside the surf-zone, such as those used in Equation 1, may not be universally appropriate for runup predictions. Guedes et al. (2011) lacked wave data within the surf-zone and consistent beach profile observations to determine if the tidal oscillations were due to changing beach slopes, changing wave dissipation, or a combination of both.

The objectives of this study were to further test relationships between runup, morphology, and forcing conditions in the field using a terrestrial laser scanner on an intermediate beach at the U.S. Army Corps of Engineers (USACE) Field Research Facility (FRF) pier in Duck, NC. Data from the terrestrial laser scanner are unique in that they enable simultaneous observations of both runup and important forcing variables, such as foreshore slope and wave conditions, at the base of the foreshore. Similar to Guedes et al. (2011), a strong tidal dependence in de-tided runup statistics was observed, which directly correlates with tidal variations in incident band energy at the base of the foreshore. This correlation was further altered depending on beach morphology and foreshore slope, which was observed to change hourly due to profile evolution and water level position.

METHODOLOGY: A description of the data collection methodologies, modeling approach, and experiment conditions are presented in the following sections. Some brief background is presented on prior approaches for measuring wave runup to highlight the advances of the methodology used in this study.

Runup Data Collection. Previous studies aimed at measuring wave runup and swash zone water levels were restricted to analyzing water-elevation time series of (1) the shoreward-most swash excursion using video imaging or near-bed resistance wires, (e.g., Holland et al. 1995; Guza and Thornton 1982), or (2) the free water surface position at a particular location on the foreshore using pressure sensors (Raubenheimer and Guza 1996). Recently, approaches using lidar technology have been developed, which allow for simultaneous, high-frequency observations of the complete free-surface and beach/swash profile position (Brodie et al. 2010; Blenkinsopp et al. 2010).

The basic premise of lidar technology is that the scanner transmits a pulsed light beam at a known angle in the direction of a target and records the time of travel between the incident and reflected pulses to determine the distance to the target, and when combined with the known angle of the pulse, calculates elevation. To scan along a narrow vertical profile, termed "line-scan," the laser beam is vertically deflected by a polygon of spinning mirrors that either continuously rotates or oscillates up and down depending upon the desired scan rate. The laser can also provide complete 360° horizontal coverage by rotating the optical head, termed "frame-scan."

For this experiment, a Riegl terrestrial laser scanner (LMS-z390i 1550µm laser) was mounted on a 4 m guyed scaffolding tower on the crest of the primary dune roughly 400 m north of the FRF pier in line with the FRF's cross-shore array of wave gauges (Hanson et al. 2010), Figure 1A. The instrument is positioned approximately 8 m above mean sea level. The laser is automated to complete an hourly 20 minute cross-shore line-scan at 2.5Hz and a 0.05° angular resolution, followed by a 180° frame scan. Twenty minute collections were chosen to be similar to the commonly used Argus eighteen minute collection length (Lippmann and Holman 1989); however, this collection length may have prevented inclusion of longer period infragravity waves in this analysis. Since the laser's vertical field of view is +/- 40° from horizontal, it is mounted at a 30° angle toward the ocean to enable viewing of the dune toe. Though angles of incidence to the water are relatively low from the laser's position on the dune, the laser reflects well off of the water surface when foam is present (blue dots, Figure 1B). Maximum range of measurement depends upon the amount of breaking and foam present in the surf-zone at any given time, but rarely exceeds 150 m for this laser scanner. Drawbacks to the laser include attenuation in heavy rain or fog, and shadowing of the backside of incoming waves due to the low grazing angle, which therefore requires interpolation to generate the full free-surface profile. In addition, returns can be sparser on the foreshore immediately following rundown when a thin film of water is left on the beach surface. Field precision and accuracy are found to be roughly twice manufacturer specifications at 0.015 m.

To extract foreshore slope, runup, and wave statistics, the remainder of this paper focuses mainly on hourly line scans. Data are first transformed from the scanner's own coordinate system (angle, range space) to rectified Cartesian coordinates (local FRF coordinates for the horizontal, and the North American Vertical Datum of 1988 (NAVD88) coordinates for the vertical), using rotation matrices determined from scans of reflectors with precisely known coordinates. Profile data are then interpolated to 10-cm resolution in the cross-shore at each time-step. To separate foreshore position from the free-surface position at each time-step, a 1.2 sec through 30 sec running minimum foreshore within each 20 minute time series is calculated, and data points are classified as water if they are >0.015 m above the running minimum foreshore (Figure 2). A running minimum foreshore is used due to foreshore elevation changes that occur on the timescale of incident and infragravity band swash (Howd and

Holman 1987). The runup time series is therefore defined using the most landward water point at each time-step (Figure 2).

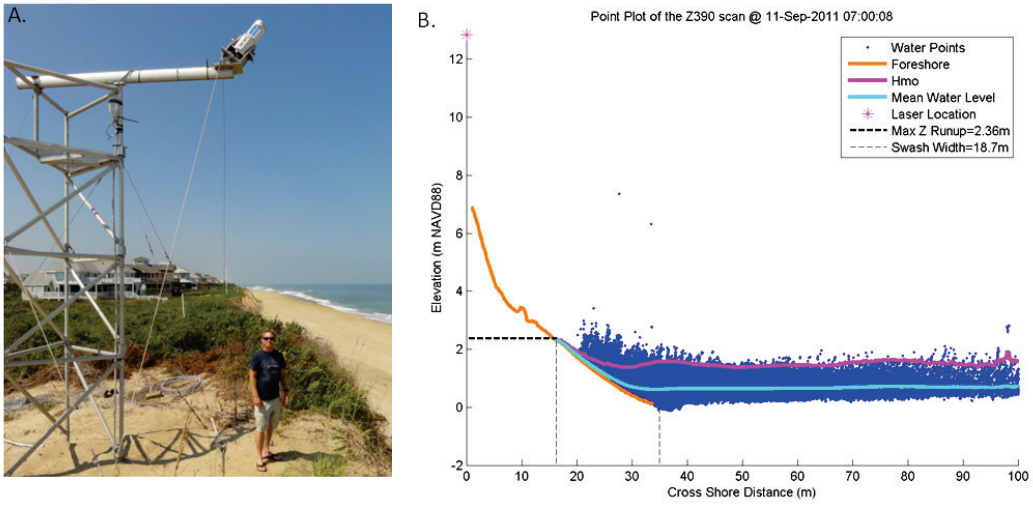

Figure 1. The laser is shown mounted in the dune in panel A, and an example of laser returns off the water surface (blue dots) over twenty minutes is shown in panel B.

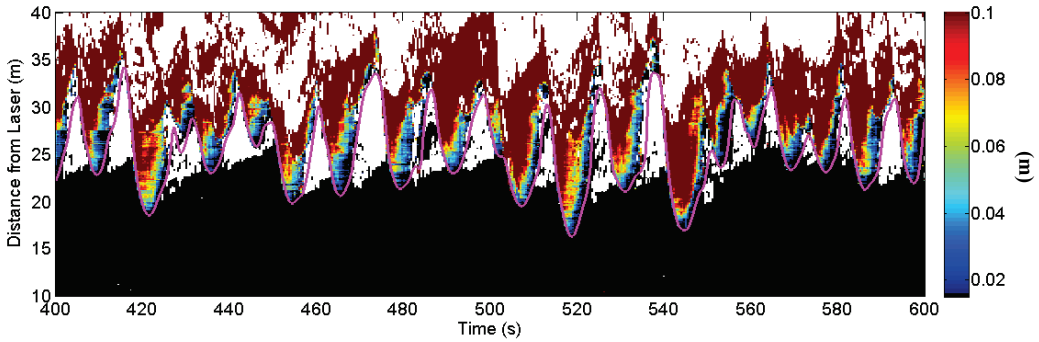

Figure 2. An example laser time stack with digitized runup time series. Colors show elevation difference from minimum foreshore. Points with elevation differences < 0.015 m are colored black. Laser data offshore of the minimum foreshore are colored red for less confusion. The runup line is shown in magenta.

Surge and tide are removed from runup time series by subtracting elevations recorded by the National Oceanic and Atmospheric Administration (NOAA) tide gauge on the end of the FRF pier where wave setup is not present. The resultant wave-driven swash is then averaged to find η_r. Spectra are also calculated on the wave-driven runup time series to find significant infragravity band swash, S_{Sig}, and significant incident band swash, S_{Sin}. In addition, observed R_2 is calculated for each runup time series based on the method described by Stockdon et al. 2006. Wave setup (η_w) and spectra are also calculated at the base of the foreshore, defined as the position of minimum rundown during the 20 minute line-scan, for each collection. These wave spectra are analyzed to calculate significant infragravity band wave height, H_{Sig}, and significant incident band wave height, H_{Sin}, and describe the hydrodynamic conditions immediately seaward of the swash zone. As described in Stockdon et al. (2006), β_f is calculated for each time-step by fitting a linear trend to the mean beach topography during each 20 minute line-scan between the location of the mean-swash +/- two swash standard deviations in the cross-shore. Cross-shore variations in beach slope were calculated by taking the first derivative down the 20 minute averaged beach profile and used to investigate beach concavity at each time-step.

Empirical Modeling Approach. For comparison to observed data, Equation 1 was calculated for each time-step twice—once using the observed beach slope and once using a "mean beach slope" for the entire experiment, to determine the sensitivity of the equation to the correct beach slope input. Wave parameters (*Ho,Lo*) were determined by reverse-shoaling data from the FRF's 11 m Acoustic Wave and Current (AWAC) profiler to deep water values. Local water levels (tide and surge) were measured at NOAA's tide station on the end of the FRF pier. Degrees of freedom for correlation analyses were calculated by dividing the total number of samples by 12 to conservatively address any issues of temporal autocorrelation within the time series.

Experiment Conditions. Analyzed data spanned a period of roughly 650 hours of semi-continuous laser observations from 26 Aug through 29 Sep 2011, including the landfall of Hurricane Irene and offshore swell from Hurricane Katia and Tropical Storm Maria, and from 26 Oct through 13 Nov 2011, during the arrival of multiple nor'easters. Wave conditions during the experiment as recorded by the 11 m AWAC at the FRF are shown in Figure 3, with red shading indicating laser collection times. Though time gaps exist in the data set, for ease of plotting, most graphs herein will show collection number rather than time on the x-axis, and vertical magenta bars will represent breaks in time (Figure 3B).

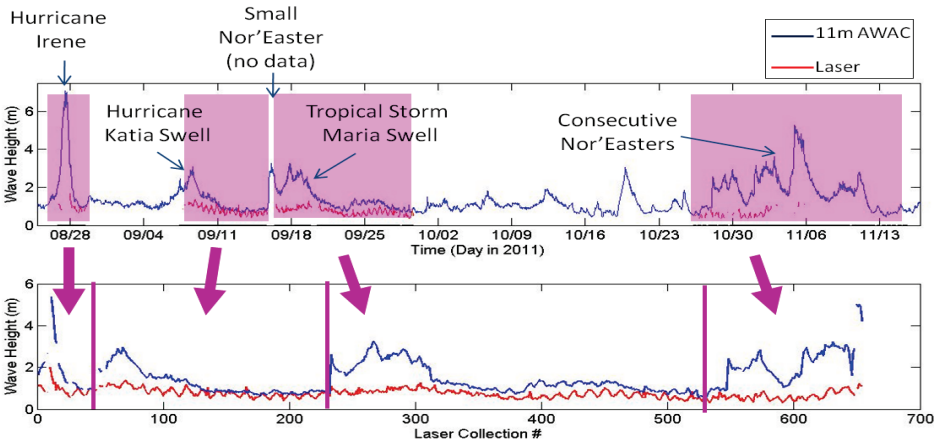

Figure 3. Wave height at the 11 m AWAC (blue) and from the laser (red) is shown in the top panel with time on the x-axis, and again in the bottom panel with laser collection number.

RESULTS: Experiment results are presented in the following sections. Morphology changes to the beach profile are discussed in the first section, with a specific concentration on variations in observed foreshore slope. Wave observations from offshore and at the base of the foreshore are discussed next, followed by modeled and observed swash data.

Foreshore Slope. Changes in foreshore slope during the course of the experiment are analyzed in Figure 4. It is important to note that the cross-shore area over which foreshore slope is calculated can change depending upon the location of the swash zone, and therefore changes in foreshore slope can be due to one of two processes (or a combination of both): (1) changes in tide level allowing the swash to cover a steeper or flatter portion of the beach or (2) bed-level changes in the foreshore due to erosion and accretion.

Mean foreshore slope during the experiment was 0.1 m/m, with values ranging from 0.02 m/m up to 0.22 m/m (or a range of 11.3°). A strong positive correlation is measured between water level and foreshore slope during the first 275 laser collections (blue line, Figure 4A), in which steeper slopes are observed at higher tides, and flatter slopes are observed at lower tides. During collections 275 through 350, little relationship between foreshore slope and water level is observed. Beginning at collection 350 and continuing to collection 450, foreshore slope variation is out of phase with the tide, such that flatter

slopes are observed at high tide and steeper slopes at low tide, though the variations in slope are less. From collection 450 through 550 and 600 through the end of the experiment, the relationship returns to in-phase.

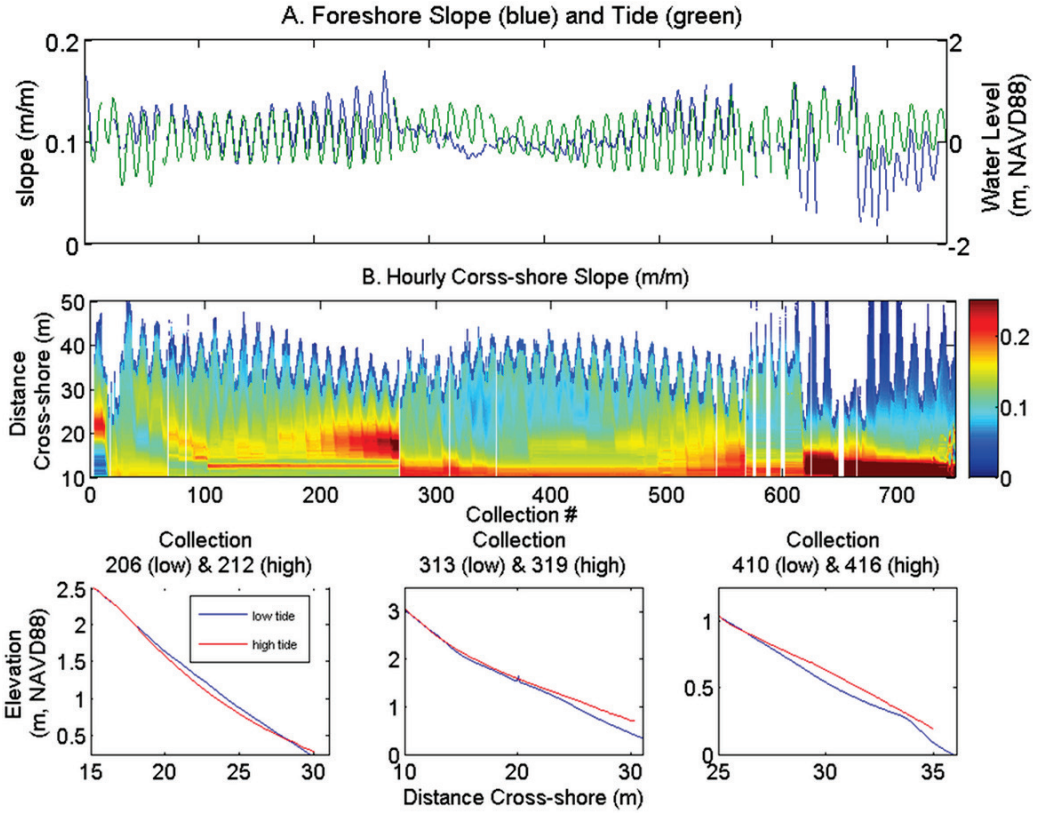

Figure 4. Analysis of changes in foreshore slope during the experiment. Foreshore slope and tide elevation are shown in panel A. In panel B, a time stack of cross-shore variations in slope is shown with warmer colors representing steeper slopes and cooler colors representing flatter slopes. In panels C-E, example profiles from low and high tide are shown.

To better illustrate these variations in foreshore slope, hourly cross-shore beach slopes (colors) are plotted in a time stack in Figure 4B, and example high and low tide profiles are plotted in Figure 4C-E. During the periods of strong in-phase correlations with water level, the beach was both (1) convex in shape—steeper slopes (warm colors) higher on the beach, and flatter slopes (cool colors) lower on the beach (Figure 4B), and (2) became even more convex at high tide due to erosion of the upper foreshore with the rising tide (red line, Figure 4C). When a lack of relationship with water level was observed, the foreshore was more linear; while accretion did occur with the rising tide, magnitudes were smaller and more evenly distributed across the profile (Figure 4D). Finally, during periods of weak out-of-phase relationship between the tide and foreshore slope, accretion occurred with the rising tide on the middle and lower foreshore. This caused the slightly concave low tide profile (blue line, Figure 4E) to become slightly convex at high tide (red line, Figure 4E).

Observed Wave Data. Offshore wave forcing parameters (*sqrt(HoLo)*) are plotted in Figure 5A. Waves during Hurricane Irene (collections 1–50) and from the offshore passage of Hurricane Katia (collections 50–80) as well as during the nor'easters at the end of the experiment (collections 600–650) were characterized by high values of *sqrt(HoLo)*, and thus strong potential for high runup and increased breaking in the surf-zone.

Hourly and 12 hour averaged measurements of de-tided η_w at the base of the foreshore (skinny and thick blue lines, respectively) are plotted with tide (dotted black line) in Figure 5B. Interestingly, a tidal signal was observed in de-tided η_w that was roughly 90° out of phase with the tide: elevated η_w (setup) was observed at mid-falling tide, whereas lower η_w and, in some cases, negative η_w (setdown) was observed at mid-rising tide. Averaging over these tidal variations suggests setup at the base of the foreshore was greatest during the nor'easters at the end of the experiment, and only slightly enhanced during Hurricane Irene and Katia waves.

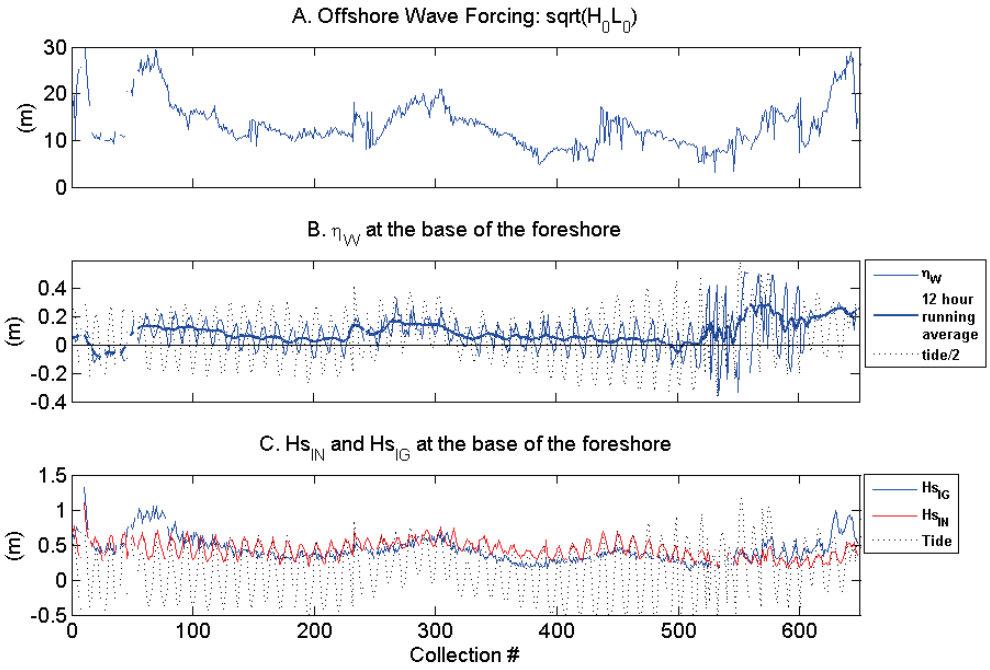

Figure 5. Offshore wave forcing from the 11 m AWAC (panel A), laser-observed water level (panel B), and wave height characteristics (panel C) at the base of the foreshore are plotted with tides during the experiment.

Significant infragravity band wave height (blue line) and significant incident band wave height (red line) at the base of the foreshore are plotted with tides (black dotted line) in Figure 5C. H_{Sig} is highest during Hurricanes Irene and Katia, and shows slight increases during Tropical Storm Maria swell and the nor'easters at the end of the experiment, similar to *sqrt(HoLo)*, as expected. A strong tidal signal is observed in H_{Sin} that is in phase with the tide and consistent with a tidally-modulated, saturated wave field, such that H_{Sin} is larger at high water level than at low water level for a given offshore wave height.

Modeled and Observed Swash Statistics. Runup predictions using offshore waves and foreshore slope measurements are shown in Figure 6A, along with phase-locked modeled (red and black lines), observed (blue line), R_2, and water level. Wave-driven runup was highest during Hurricanes Irene and Katia, and during the nor'easters at the end of the experiment. A strong in-phase tidal signal is apparent in de-tided, observed, R_2 such that R_2 is higher at high tide than low tide for a given offshore wave condition. This tidal signal is only apparent in the model data when the observed foreshore slope is included (red line), and therefore during periods of time when foreshore slope was not strongly correlated with water level (Figure 4A), no tidal variation was predicted by Equation 1. While including observations of foreshore slope in Equation 1 increased the correlation between predicted and observed data from an $r^2 = 0.36$ ($p<<0.001$) to an $r^2 = 0.56$ ($p<<0.001$), however, inclusion of slope variation alone does not result in sufficient tidal modulation when compared with measurements.

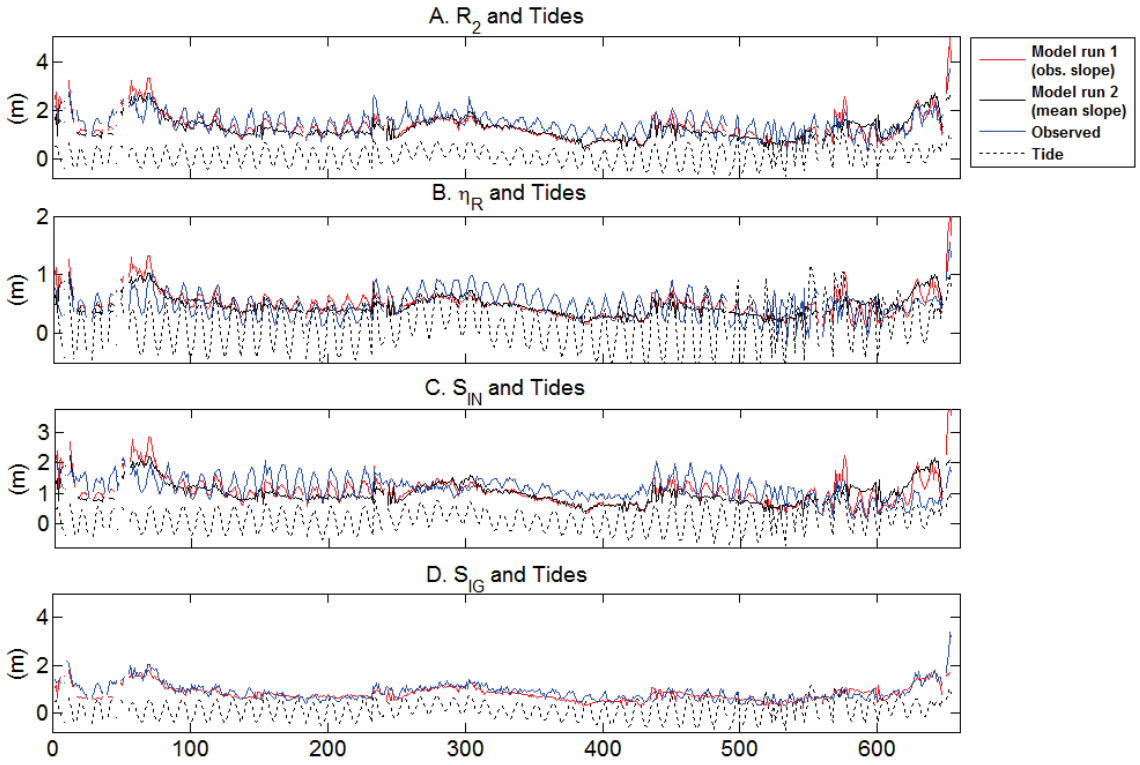

Figure 6. Observed and modeled swash statistics plotted with tides during the experiment. The laser collection number is shown on the x-axis.

The results for η_R are similar to those of R_2, with a strong in-phase relationship between observed data and water level that was not predicted by Equation 1. In addition, a significant correlation between observed data and tidal elevation exists for S_{IN}, with the exception of collection numbers 250–450, where the relationship mirrors that of foreshore slope and tides (Figure 4A). In general, there seems to be little tidal dependence in S_{IG}, which instead correlates well with $sqrt(H_oL_o)$ ($r^2=0.65$, $p<<0.001$).

DISCUSSION: The above results are discussed in the following sections with a focus on understanding the observed tidal variations in many of the measured variables. The results suggest that increased or decreased breaking over the sandbar at low and high tides, respectively, may modulate energy in the incident band, affecting runup at the shoreline. The implications of this sandbar filtering are (1) that up-to-date bathymetry or a quantification of dissipation across the surf-zone in addition to sub-aerial beach morphology is necessary to produce accurate runup predictions that capture alongshore variations along the coastline. A new equation for predicting wave runup is proposed that includes incident band wave-height at the base of the foreshore with beach foreshore slope and offshore wave parameters, and it explains 73% of the variance in the observations. The feasibility of using this equation in practice is also addressed.

Foreshore Slope. Changes in both erosion/accretion and the cross-shore position of the swash with the rising and falling tide, as well as changing wave conditions, can contribute to the hourly evolution of foreshore slope on intermediate beaches. In this experiment, the relationship between erosion and accretion patterns and the rising and falling tide changed depending upon the shape of the beach. A concave beach that featured steep slopes on the upper foreshore and flatter slopes on the lower foreshore was further eroded during the rising tide, creating even steeper slopes in the swash zone. In contrast, a slightly convex beach that featured flatter, upper foreshore slopes and steeper, lower foreshore slopes

tended to accrete with the rising tide, creating even flatter slopes within the high tide swash zone. Linear beaches tended to accrete and erode more uniformly with the rising and falling tide.

Though profile elevation changes were only on the order of +/- 0.15 m, and the mean cross-shore position of the swash only varied by roughly 10m from high tide to low tide, changes in slope during in-phase collection times (convex beach) often reached 4°, a change of ~70° of the mean beach slope. Surprisingly, a change in 4° of slope will change the runup predictions made by Equation 1 by 47%, which highlights the potential errors in using Equation 1 when the current beach foreshore slope is not known.

Wave Climate at the Base of the Foreshore. Significant wave height in the incident band at the base of the foreshore oscillated strongly with the tides, such that higher H_{Sin} were observed at high-tides and lower H_{Sin} were observed at low-tide for the same given offshore wave conditions. Video imagery collected by the Argus cameras at the FRF was used to investigate wave breaking in the surf-zone as a possible explanation of this. An example set of imagery is shown from 28 Sep 2011 at high tide (Figure 7A) and low tide (Figure 7B), with the location of the lidar profile in magenta. The image is a "bright" image, which saves the brightest intensity at each pixel during the hourly Argus collection, and thus maps regions of wave breaking (white pixels) in the surf-zone. As seen in panel A, at high tide there is a small amount of breaking over the nearshore sandbar, and a wide, energetic swash zone is observed on the beach. In contrast, at low tide, there is significantly increased breaking over the sandbar (due to lower water levels), and a more narrow swash zone can be seen on the beach. This supports wave data from the lidar, which indicated lower wave heights at the base of the foreshore at low tide. These observations suggest that increased breaking of incident band waves at low tide over the offshore sandbar decreases the amount of incident band energy reaching the shoreline, supporting one hypothesis proposed by Guedes et al. (2011). Interestingly, neither *Hsig* nor SIG correlates with water level, even though increased breaking at low tide should promote the release of infragravity band waves (Ruessink 1998).

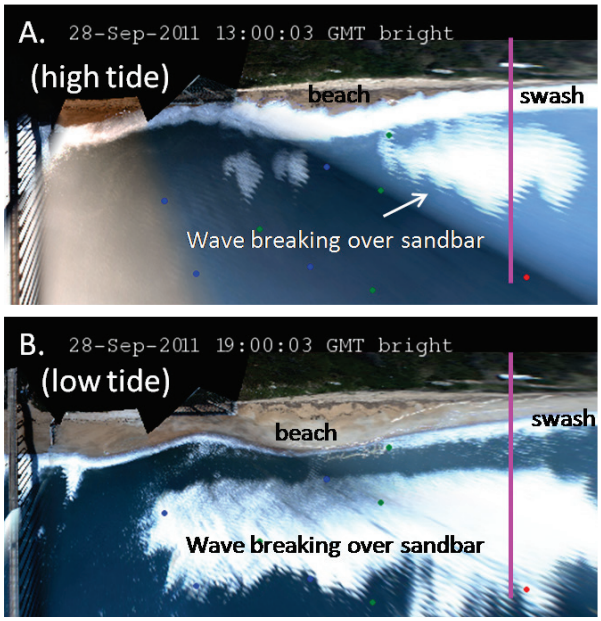

Figure 7. Argus' brightest pixel images for a high tide (A) and subsequent low tide (B) showing variations in wave breaking in the surf-zone.

Though ηw at the base of the foreshore did show a strong tidal oscillation, it was roughly 90° out of phase with the tide, having peaks at mid-falling tide and valleys at mid-rising tide. This suggests that the

rapid increase of setup at the shoreline may begin slightly farther offshore during low and rising tides, whereas at high and falling tides, wave shoaling in the shore break at the base of the foreshore may actually create a slight setdown in water levels before the rapid rise in the swash. Changes in wave shape and the development and movement of a shoreline "step" feature during the rising and falling tides (Bauer and Allen 1995) may also contribute to these observed patterns.

Runup Predictions. Though R_2 predictions from Equation 1 were improved when observed changes in beach slope were included on an hourly basis, it still only explained 54% of the variance in the observed R_2 data, and could not reproduce the observed tidally dominated variation in runup when beach slope was not in phase with the tide. Examination of Equation 1 reveals that the only functional dependence of runup on water level is through the inclusion of the foreshore slope parameter, because the remaining forcing parameters are based on deep water wave height. However, as described above, the data instead suggest that the incident band wave conditions at the base of the foreshore dominate runup variations on an intermediate beach. Specifically, the data show that wave conditions at the base of the foreshore can change with water level independently of the offshore wave conditions, before interacting with the foreshore, due to shallow-depth driven wave breaking.

To quantify these observations and their effect on runup, observed R_2 was deconstructed into observed ηR, S_{IN}, and S_{IG} (similar to the approach of Equation 1) and these variables compared with forcing parameters measured at the foreshore (Bf and H_{Sin}) and offshore ($sqrt(HoLo)$). Specifically, η_R showed a positive correlation with H_{Sin} ($r^2 = 0.5$, $p<<0.001$), S_{IN}, showed a strong positive correlation to $H_{Sin}B_f$ ($r2 = 0.73$, $p<<0.001$), and S_{IG} showed a strong positive correlation to $sqrt(HoLo)$ ($r^2 = 0.66$, $p<<0.001$). Combining these relationships in a similar way to Stockdon et al. (2006), yields a new equation for runup:

$$R_2 = 1.1\left\{0.8Hs_{IN} + \frac{\sqrt{\left(25Hs_{IN}B_f\right)^2+\left(0.06\sqrt{H_0L_0}\right)^2}}{2}\right\}. \quad \text{Eq. 2}$$

A scatter plot of predicted R_2 with Equation 2 and observed R_2 is shown in Figure 8. Equation 2 explains 73% of the variance in observed R_2, compared to Equation 1, which only explained 56% of the variance. In addition, removing the dependence on the highly variable parameter, Bf, and altering the coefficient before H_{Sin} in the S_{IN} component from 25 to 2.5 in Equation 2, explains 69% of the variance in observed R_2. While knowing beach slope is still important in runup predictions, this suggests that runup can be almost as well predicted by only knowing the morphology of the surf-zone and its effect on wave energy reaching the beach. In fact, Equation 2, without including beach slope, explained more of the variance in wave runup during the experiment when compared with the commonly used Equation 1.

Wave height in the incident band at the base of the foreshore is rarely known, and thus Equation 2 may not be practical for predictive use; however, it better represents the physical drivers of runup, particularly on barred intermediate beaches. A more readily available remotely sensed variable, such as a measure of wave breaking and bar morphology from video or radar imagery, could be investigated for use as a scaling factor to convert offshore wave parameters to H_{Sin} at the base of the foreshore, making Equation 2 more readily applicable.

Implications for Alongshore Variations in Runup and Inundation. This study did not specifically address alongshore variations in runup, however, the temporal variations observed can be translated to provide a possible explanation of the correlation between sandbar morphology and beach erosion observed by Brodie and McNinch (2011). Specifically, this study illustrated how temporal variations in wave breaking over a sandbar during the course of a tidal cycle in combination with the shape of the beach could create temporal variations in wave runup for a constant offshore wave height. Similarly, alongshore variations in sandbar configuration will dissipate different amounts of wave

energy, creating alongshore variations in the amount of wave energy that reaches the beach, even though the offshore wave conditions may be the same along the coastline. Small-scale alongshore variations in the slope and curvature of the beach can then further enhance or inhibit runup, creating more alongshore variation in runup. A schematic summarizing this concept is presented in Figure 9, where panel A depicts a multiple-barred stretch of beach with increased wave dissipation through the surf-zone and less runup. Panel B depicts steeper surf-zone morphology with less breaking over a single bar and more energy reaching the shoreline and interacting with a steep beach, ultimately leading to higher runup and increased potential for erosion. Therefore, current observations or model predictions of the antecedent morphology are paramount to being able to correctly predict runup inundation and refine vulnerability assessments immediately prior to a specific storm threat.

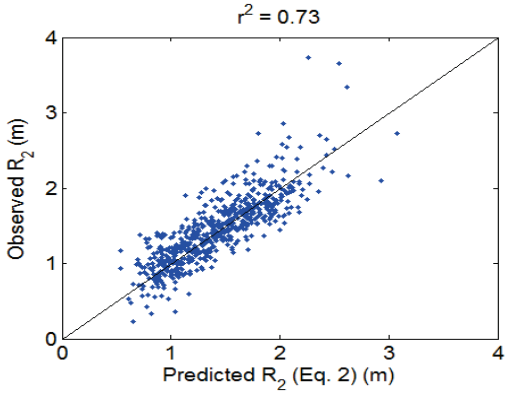

Figure 8. Example GIS window showing spatial SSURGO soils data on top of FAO soils data, along with the FAO soil attributes.

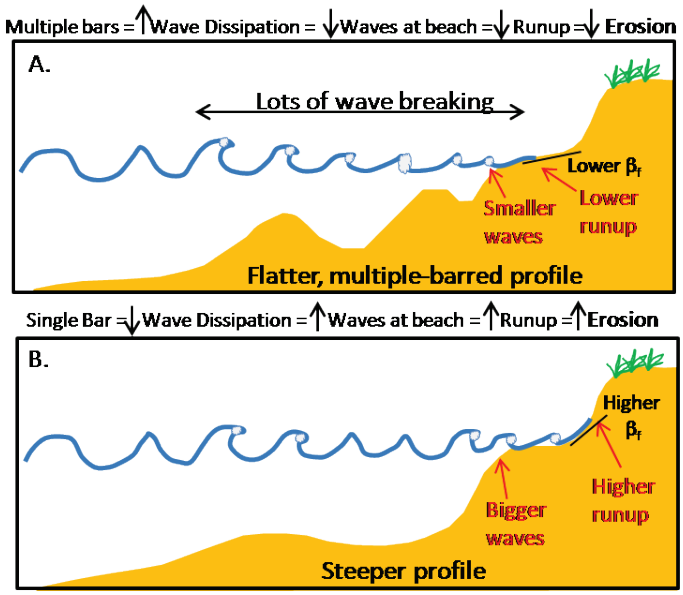

Figure 9. Diagram showing effect of surf-zone and beach morphology on wave dissipation and runup.

CONCLUSIONS: A dune-mounted terrestrial laser scanner was used to make hourly observations of beach morphology, swash, and inner surf-zone hydrodynamics to investigate the physical drivers of runup on an intermediate beach under a variety of wave conditions. Data revealed a strong tidal signal in both, the wave height at the base of the foreshore and the resultant de-tided 2% exceedence observations of runup. Specifically, mean and incident band swash, as well as incident band wave height at the base

of the foreshore were observed to oscillate in-phase with the tide, such that for a given offshore wave condition, all were elevated at high tide relative to low tide. Coincident video imagery suggested that this was primarily due to increased breaking of incident band waves at low tide over a nearshore bar, which dissipated wave energy. Based on these relationships, a new equation was developed (Equation 2), and shown to explain 20% more of the variance in observed R_2 when compared with the commonly used Stockdon et al. (2006) equation (Equation 1). Equation 1 appeared overly sensitive to changes in beach slope, which was observed to change by as much as 4° from high tide to low tide and 11° over the course of the entire experiment. Changes in foreshore slope were due to small-scale profile adjustments with tide (erosion and accretion on the order of +/- 0.15 m) and were either in phase with the tide (concave profiles), 180° out of phase with the tide (convex profiles), or independent of the tide (linear profiles). Interestingly, even though beach slope was highly variable throughout the experiment, removing it from Equation 2 only reduced r^2 values by 6%, suggesting that changes to the wave climate across the surf-zone may have a larger effect on runup, than variations in beach slope.

These data, in combination with prior work (Brodie et al. 2011), suggest that knowledge of the morphology of the profile and surf-zone immediately prior to an approaching event is critical for producing correct predictions of wave-driven runup during storms. Furthermore, extreme or long-duration events frequently cause significant morphological evolution to the system, which, in turn, may alter runup predictions during the storm. Therefore, effort should also be focused on using numerical models, such as CSHORE (Kobayashi 2009), to model the potential morphological changes to the system, so that runup predictions remain accurate throughout the course of an event.

ADDITIONAL INFORMATION: For additional information, contact Kate L. Brodie, Coastal Observation and Analysis Branch, Coastal Hydraulics Laboratory by mail at 1261 Duck Rd, Duck, NC 27949; by phone at 252-261-6840 extension 233; or via email: Katherine.L.Brodie@usace.army.mil.

This CHETN should be cited as follows:

> Brodie, K. L. 2016. *Importance of antecedent beach and surf-zone morphology to wave runup predictions*. Coastal and Hydraulics Engineering Technical Note. ERDC/CHL CHETN-I-92. Vicksburg, MS: U.S. Army Engineer Research and Development Center. *http://chl.erdc.usace.army.mil/chetn*.

REFERENCES

Bauer, B. O., and J. R. Allen. 1995. Beach steps: An evolutionary perspective. Marine Geology 123(3): 436—166.

Blenkinsopp, C. E., M. A. Mole, I. L. Turner, and W. L. Pierson. 2010. Measurements of the time-varying free-surface profile across the swash zone obtained using an industrial LIDAR. Coastal Engineering 57(11): 1059–1065.

Brodie, K. L., J. E. McNinch, M. Forte, and R. Slocum. 2010. Low-grazing angle laser scans of foreshore topography, swash and inner surf-zone wave heights, and mean water level: validation and storm response. AGU Fall Meeting Abstracts 1:04.

Brodie, K. L., and J. E. McNinch. 2011. Beach change during a nor'easter: relationships to wave steepness and inner surf-zone dissipation. In Proceedings of Coastal Sediments 2011, 2—6 May, Miami, Florida, eds. J.D. Rosati, P. Wang, and T.M. Roberts, 1360–1374.

Guedes, R. M. C., K. R. Bryan, G. Coco, and R. A. Holman. 2011. The effects of tides on swash statistics on an intermediate beach. Journal of Geophysical Research: Oceans 116 (C4).

Guza, R. T., and E. B. Thornton. 1982. Swash oscillations on a natural beach. Journal of Geophysical Research: Oceans 87(C1): 483–491.

Guza, R. T., and E. B. Thornton. 1981. Wave set-up on a natural beach. Journal of Geophysical Research 86(C5): 4133–4137.

Hanson, J. L., H. C. Friebel, and K. K. Hathaway. 2010. Coastal wave transformation: Observations and modeling. In Proceedings, The 17th Waves in Shallow water Environment Meeting (WISE '10), 25—29 April, Brest France.

Holland, K. T., B. Raubenheimer, R. T. Guza, and R. A. Holman. 1995. Runup kinematics on a natural beach. Journal of Geophysical Research: Oceans 100(C3): 4985–4993.

Holland, K. T., and J. A. Puleo. 2001. Variable swash motions associated with foreshore profile change. Journal of Geophysical Research: Oceans 106(C3): 4613–4623.

Holland, K.T., and R.A. Holman. 1993. The statistical distribution of swash maxima on natural beaches. Journal of Geophysical Research: Oceans 98(C6): 10271–10278.

Holman, R. A. 1986. Extreme value statistics for wave run-up on a natural beach. Coastal Engineering 9(6): 527–544.

Holman, R. A., and A. H. Sallenger, Jr. 1985. Setup and swash on a natural beach. J. Geophys. Res.: Oceans 90(C1): 945–953.

Howd ,P. A., and R. A. Holman. 1987. A simple model of beach foreshore response to long-period waves. Marine Geology 78(1-2): 11–22.

Kobayashi, N. 2009. Documentation of cross-shore numerical model CSHORE. Research Report No. CACR-09-06. Newark, DE: University of Delaware, Center for Applied Coastal Research.

Lippmann, T. C., and R. A. Holman. 1989. Quantification of sand bar morphology: A video technique based on wave dissipation. Journal of Geophysical Research: Oceans 94(C1): 995–1011.

Longuet-Higgins, M. S., and R. W. Stewart R. W. 1964. Radiation stresses in water waves; a physical discussion, with applications. Deep Sea Research and Oceanographic Abstracts 11(4): 529–562.

Masselink, G., and M. Hughes. 1998. Field investigation of sediment transport in the swash zone. Continental Shelf Research 18(10): 1179–1199.

Melby, J. A. 2012. Wave runup prediction for flood hazard assessment. ERDC/CHL TR-12-24. Vicksburg MS: U.S. Army Engineer Research and Development Center.

Nielsen, P., and D. J. Hanslow. 1991. Wave runup distributions on natural beaches. Journal of Coastal Research 7(4): 1139–1152.

Plant, N. G., H. F. Stockdon, A. H. Sallenger, Jr., M. J. Turco, J. W. East, A. A. Taylor, and W. A. Shaffer. 2010. Forecasting hurricane impact on coastal topography. Eos, Transactions American Geophysical Union 91(7): 65–72.

Raubenheimer, B., and R. T. Guza. 1996. Observations and predictions of run-up. Journal of Geophysical Research: Oceans 101(C11): 25575–25587.

Ruessink, B. G. 1998. The temporal and spatial variability of infragravity energy in a barred nearshore zone. Continental Shelf Research 18(6): 585–605.

Ruessink, B. G., M. G. Kleinhans, and P .G. L. van den Beukel. 1998. Observations of swash under highly dissipative conditions. Journal of Geophysical Research: Oceans 103(C2): 3111–3118.

Ruggiero, P. 2004. Wave run-up on a high-energy dissipative beach. Journal of Geophysical Research: Oceans 109(C6).

Sallenger, Jr., A. H. 2000. Storm impact scale for barrier islands. Journal of Coastal Research 16(3): 890–895.

Stockdon, H. F., A. H. Sallenger, Jr., R. A. Holman, and P. A. Howd 2007. A simple model for the spatially-variable coastal response to hurricanes. Marine Geology 238(1): 1–20.

Stockdon. H. F., R. A. Holman, P. A. Howd, and A. H. Sallenger Jr. 2006. Empirical parameterization of setup, swash, and runup. Coastal Engineering 53(7): 573–588.